

On the crystallinity of silicate dust in evolving protoplanetary disks due to magnetically driven disk winds

SOTA ARAKAWA ¹, YUJI MATSUMOTO ² AND MITSUHIKO HONDA ³

¹*Division of Science, National Astronomical Observatory of Japan
2-21-1 Osawa, Mitaka, Tokyo 181-8588, Japan.*

²*Center for Computational Astrophysics, National Astronomical Observatory of Japan
2-21-1 Osawa, Mitaka, Tokyo 181-8588, Japan.*

³*Faculty of Biosphere–Geosphere Science, Okayama University of Science
1-1 Ridai-chou, Okayama 700-0005, Japan.*

Submitted to ApJ

ABSTRACT

We present a novel mechanism for the outward transport of crystalline dust particles: the outward radial drift of pebbles. The dust ring structure is frequently observed in protoplanetary disks. One of the plausible mechanisms of the formation of dust rings is the accumulation of pebbles around the pressure maximum, which is formed by the mass loss due to magnetically driven disk winds. In evolving protoplanetary disks due to magnetically driven disk winds, dust particles can migrate outwardly from the crystallization front to the pressure maximum by radial drift. We found that the outward radial drift process can transport crystalline dust particles efficiently when the radial drift timescale is shorter than the advection timescale. Our model predicts that the crystallinity of silicate dust particles could be as high as 100% inside the dust ring position.

1. INTRODUCTION

Protoplanetary disks are the birth places of planetary systems. Therefore, disk evolution is of great importance to understand how planets formed (e.g., [Testi et al. 2014](#)). As planetesimal formation via accumulation of dust particles is the first step of planet formation (e.g., [Johansen et al. 2014](#)), the spatial distribution and migration of dust particles in evolving protoplanetary disks have been studied extensively so far.

Several pieces of evidence suggest that silicate dust undergoes significant thermal processing in protoplanetary disks. In the interstellar medium, silicate dust is thought to be completely amorphous, as suggested by broad and smooth absorption features (e.g., [Kemper et al. 2004](#)). In contrast, crystalline silicate features are often found toward disks around Herbig Ae/Be stars (e.g., [Hanner et al. 1995](#)) and T Tauri stars (e.g., [Honda et al. 2003, 2006](#)). Forsterite (Mg_2SiO_4) is the most abundant silicate mineral in disks (e.g., [Juhász et al. 2010; Maaskant et al. 2015](#)). Laboratory experiments suggest that the crystallization temperature of forsterite is approximately 600–1000 K (e.g., [Hallenbeck et al. 2000; Yamamoto & Tachibana 2018](#)). However, in some disks around young stars, crystalline forsterite has been observed much farther

away from the “crystallization front”, where the disk temperature is equal to the crystallization temperature (e.g., [Juhász et al. 2010; de Vries et al. 2012; Sturm et al. 2013](#)). In addition, comets and interplanetary dust particles in our solar system contain crystalline silicate (e.g., [Honda et al. 2004; Ootsubo et al. 2007; Ogliore et al. 2009](#)). These facts strongly suggest that the crystallization and outward transport processes occurred both in extrasolar protoplanetary disks and in the early solar nebula.

Several mechanisms have been suggested as driving the outward transport of crystalline dust particles in protoplanetary disks, including turbulent diffusion (e.g., [Gail 2001; Ciesla 2010](#)), large-scale circulations associated with mass and angular momentum transfer (e.g., [Keller & Gail 2004; Ciesla 2007, 2009](#)), spiral arms in gravitationally unstable massive disks (e.g., [Boss 2008](#)), photophoresis (e.g., [Mousis et al. 2007](#)), and radiation pressure (e.g., [Vinković 2009; Tazaki & Nomura 2015](#)). [Dullemond et al. \(2006\)](#) proposed that the majority of crystalline dust particles are formed in the very early phase of disk formation via the collapse of molecular cloud cores (see also [Yang & Ciesla 2012](#)). In addition, parts of crystalline dust particles might be formed in-situ in the outer region of protoplanetary disks by exothermic chemical reactions of reactive molecules ([Tanaka et al. 2010](#)) and/or by shock waves (e.g., [Harker & Desch 2002; Miura et al. 2010](#)).

The physical process of outward transport by turbulence is described by the diffusion equation. The key parameter for turbulent mixing in steady state disks is the Schmidt number, which is the ratio of the kinetic viscosity and diffusion coefficient (e.g., [Clarke & Pringle 1988](#)). [Pavlyuchenkov & Dullemond \(2007\)](#) reviewed how the Schmidt number affects the crystallinity of disks. They found that the radial distribution of the crystallinity in steady state disks is given by a power-law distribution, and the exponent depends on the Schmidt number. A small value of the Schmidt number lower than one is required for efficient outward diffusion in standard accretion disks (e.g., [Clarke & Pringle 1988](#); [Pavlyuchenkov & Dullemond 2007](#); [Hughes & Armitage 2010](#)).

The radial drift of dust particles due to gas drag is another important process to understand the radial transport of dust particles. In classical views of accretion disks (e.g., [Lynden-Bell & Pringle 1974](#); [Hartmann et al. 1998](#)), the pressure gradient at the midplane is negative throughout the disk, and dust particles migrate inward due to gas drag (e.g., [Adachi et al. 1976](#)). This inward drift offsets the outward transport of dust particles (e.g., [Ciesla 2010](#)). In addition, mm- to cm-sized large dust particles spiral into the central star within 1 Myr unless a local pressure maximum prevents the dust particles from inward migration (e.g., [Desch et al. 2018](#); [Fukai & Arakawa 2021](#)). Therefore, it is difficult for standard accretion disks to transport dust particles formed at high temperatures outwardly and to maintain high crystallinity for a long time in the outer region. We briefly review the effect of radial drift on the radial distribution of the crystallinity in Section 3.1.

Recent astronomical observations have revealed varieties of structures of protoplanetary disks (e.g., [Fukagawa et al. 2013](#); [ALMA Partnership et al. 2015](#); [Tsukagoshi et al. 2016](#); [van Boekel et al. 2017](#); [Andrews et al. 2018](#)). The observed disk structures provide us plenty of clues to reveal how planets formed (see [Andrews 2020](#), and references therein). In particular, the dust ring structure is observed in a large number of disks. To date, several mechanisms are proposed for the origin: planets (e.g., [Dong et al. 2015](#); [Kanagawa et al. 2018](#)); dust growth (e.g., [Lambrechts & Johansen 2014](#); [Ohashi et al. 2021](#)); condensation fronts (e.g., [Okuzumi et al. 2016](#); [Pinilla et al. 2017](#)); photoevaporative flows (e.g., [Ercolano & Pascucci 2017](#)); disk instabilities due to dust-gas friction and self-gravity (or turbulent gas viscosity) (e.g., [Takahashi & Inutsuka 2014](#); [Tominaga et al. 2019](#)); magnetically driven disk winds (e.g., [Takahashi & Muto 2018](#)).

In this study, we focus on the crystallinity of silicate dust particles in ring structures formed by the magnetically driven disk winds. [Suzuki & Inutsuka \(2009\)](#) found that magnetohydrodynamic turbulence in protoplanetary disks drives disk winds. [Suzuki et al. \(2010\)](#) revealed that the mass loss timescale of the magnetically driven disk winds is propor-

tional to the local Keplerian rotation period, and disk winds disperse the gas component of disks from the inner region. In other words, magnetically driven disk winds potentially create a maximum of gas pressure around 1–10 au from the central stars (e.g., [Suzuki et al. 2016](#)), and dust particles which are dynamically decoupled with gas (referred to as “pebbles”) are accumulated around the pressure maximum (e.g., [Haghighipour & Boss 2003](#)). This is the formation mechanism of dust ring in evolving disk due to disk winds proposed by [Takahashi & Muto \(2018\)](#).

In this study, we propose a novel mechanism for outward transport of crystalline dust particles. In evolving protoplanetary disks due to magnetically driven disk winds, dust particles can migrate outwardly by radial drift. We found that the *outward radial drift* process can transport crystalline dust particles efficiently when the radial drift overcomes the advective flow (see Figure 11). Our model predicts that the crystallinity of silicate dust particles could be as high as 100% inside the dust ring position, and this is totally different from the prediction for accretion disks without disk winds (e.g., [Pavlyuchenkov & Dullemond 2007](#)).

2. MODELS

In Section 2, we briefly introduce the equations used to compute the evolution of protoplanetary disks. We calculate the temporal evolution of the surface densities of gas and dust using vertically integrated disk models, and we also obtain the radial distribution of the crystallinity of dust particles. The basic equations for the evolution of gas and dust disks are described in Sections 2.1 and 2.2, respectively.

2.1. Evolution of gas disk

We set the initial distribution of the gas surface density, $\Sigma_{\text{gas},0}$, as a self-similar profile, which is described as follows ([Lynden-Bell & Pringle 1974](#)):

$$\Sigma_{\text{gas},0} = \frac{(2-\gamma)M_{\text{disk}}}{2\pi r_0^2} \left(\frac{r}{r_0}\right)^{-\gamma} \exp\left[\left(-\frac{r}{r_0}\right)^{2-\gamma}\right], \quad (1)$$

where $M_{\text{disk}} = 0.01M_{\star}$ is the total mass of the gas disk, $r_0 = 100$ au is the initial disk radius, and $\gamma = 1$ is the exponent for the gas surface density profile. Here r denotes the distance from the central star. As an example, we take a Herbig Ae/Be star with the mass of $M_{\star} = 2.5M_{\odot}$ (M_{\odot} is the solar mass) as assumed in [Pavlyuchenkov & Dullemond \(2007\)](#). For simplicity, we assume that the (midplane) temperature of the disk are given as follows:

$$T = T_1 \left(\frac{r}{1 \text{ au}}\right)^{-q}, \quad (2)$$

where $T_1 = 800$ K is the temperature at $r = 1$ au, and $q = 1/2$ is the exponent for the temperature structure. We also set the location of the crystallization front at $r_c = 1$ au, and all

dust is crystalline for $r \leq r_c$ (Pavlyuchenkov & Dullemond 2007).

The basic equation of the evolution of gas surface density of accretion disks with magnetically driven disk winds is

$$\frac{\partial \Sigma_{\text{gas}}}{\partial t} = \frac{1}{2\pi r} \frac{\partial \dot{M}_{\text{gas}}}{\partial r} + \dot{\Sigma}_{\text{wind}}, \quad (3)$$

where

$$\dot{M}_{\text{gas}} = 6\pi r^{1/2} \frac{\partial (r^{1/2} \Sigma_{\text{gas}} \nu)}{\partial r}, \quad (4)$$

is the (vertically integrated) mass flux at every location r , and $\dot{\Sigma}_{\text{wind}}$ is the mass loss rate due to the disk wind. Then, the advection velocity, v_{adv} , is

$$v_{\text{adv}} = \frac{\dot{M}_{\text{gas}}}{2\pi r \Sigma_{\text{gas}}}. \quad (5)$$

The advection velocity is positive when the gas flows inwardly.

The mass flux is proportional to the kinematic viscosity,

$$\nu = \alpha_{\text{acc}} c_s h_g, \quad (6)$$

where α_{acc} is the angular momentum transport efficiency parameter called alpha parameter (Shakura & Sunyaev 1973), c_s is the sound speed, and h_g is the gas scale height. The gas scale height, h_g , and the midplane gas density, ρ_g , are given by

$$h_g = \frac{c_s}{\Omega_K}, \quad (7)$$

$$\rho_g = \frac{\Sigma_{\text{gas}}}{\sqrt{2\pi} h_g}, \quad (8)$$

where $\Omega_K = \sqrt{GM_*/r^3}$ is the Keplerian frequency, and G is the gravitational constant.

Suzuki et al. (2010) investigated the mass loss rate due to the magnetically driven disk wind. Based on their three-dimensional local magnetohydrodynamic simulations, the mass loss rate due to the disk wind is given by

$$\dot{\Sigma}_{\text{wind}} = -C_w \Sigma_{\text{gas}} \Omega_K, \quad (9)$$

where C_w is the efficiency parameter (see also Takahashi & Muto 2018). We set the typical value of $C_w = 10^{-5}$ in Section 3.2.

Miyake et al. (2016) found that not only gas but also small dust particles can be blown out by the disk wind. However, we do not consider this effect. The dust blown-out process works when their Stokes number satisfies $\text{St} < C_w/1.8$ (Taki et al. 2021). As we set $C_w = 10^{-5}$, pebbles which can drift due to gas drag would not be blown out by the disk wind.

2.2. Motion of dust particles

We set the initial distribution of the dust surface density, $\Sigma_{\text{dust},0}$, as follows:

$$\Sigma_{\text{dust},0} = 0.01 \Sigma_{\text{gas},0}. \quad (10)$$

In this study, we consider two types of dust particles: crystalline and amorphous particles. We define the crystallinity, C , as the fraction of the crystalline dust particles:

$$C \equiv \frac{\Sigma_c}{\Sigma_{\text{dust}}}, \quad (11)$$

where Σ_c is the surface density of the crystalline dust particles, and the dust surface density is the sum of the surface densities of crystalline and amorphous particles: $\Sigma_{\text{dust}} = \Sigma_c + \Sigma_a$.

We compute the temporal evolution of the surface densities of crystalline and amorphous dust particles. We consider three physical processes: advection in the mean gas flow, diffusion due to concentration gradient, and the radial drift of dust particles relative to the gas (see Fukai & Arakawa 2021, and references therein). In addition, we also take into account the effect of conversion of dust to planetesimals via the streaming instability (see Section 2.2.3).

The surface densities of crystalline and amorphous dust particles evolve according to

$$\frac{\partial \Sigma_i}{\partial t} = \frac{1}{2\pi r} \frac{\partial \dot{M}_i}{\partial r} + \dot{\Sigma}_{\text{plts},i}, \quad (12)$$

where the subscript i denotes the crystalline ($i = c$) or amorphous ($i = a$) dust particles. The mass flux of dust particles, \dot{M}_i , is given by the sum of the three physical processes:

$$\dot{M}_i = \dot{M}_{i,\text{adv}} + \dot{M}_{i,\text{diff}} + \dot{M}_{i,\text{drift}}, \quad (13)$$

and $\dot{\Sigma}_{\text{plts},i}$ is the conversion rate of dust to planetesimals.

2.2.1. Advection, diffusion, and radial drift

Desch et al. (2017) re-derived the equations for radial transport of dust particles. The advection term is given by

$$\dot{M}_{i,\text{adv}} = 2\pi r \Sigma_i v_{\text{adv}}, \quad (14)$$

and the diffusion term is

$$\dot{M}_{i,\text{diff}} = 2\pi r \Sigma_i v_{i,\text{diff}}, \quad (15)$$

where the diffusion velocity, $v_{i,\text{diff}}$, is given by

$$v_{i,\text{diff}} = D \left(\frac{\Sigma_i}{\Sigma_{\text{gas}}} \right)^{-1} \frac{\partial}{\partial r} \left(\frac{\Sigma_i}{\Sigma_{\text{gas}}} \right). \quad (16)$$

Here D is the diffusion coefficient of the dust particles, which is given by

$$D = \frac{\nu}{\text{Sc}(1 + \text{St}^2)}, \quad (17)$$

where Sc is the Schmidt number and St is the Stokes number of the dust particles (see Section 2.2.2). The diffusion velocity is positive when the direction of the flow is inward. We note that the Stokes number is sufficiently small ($St \ll 1$) in our simulations, and the diffusion coefficient is approximately given by $D \simeq \nu/Sc$. The radial drift term is given by

$$\dot{M}_{i,\text{drift}} = 2\pi r \Sigma_i v_{\text{drift}}, \quad (18)$$

and the drift velocity, v_{drift} , is given by the following equation:

$$v_{\text{drift}} = \frac{St}{1 + St^2} (\eta r \Omega_K - St v_{\text{adv}}). \quad (19)$$

Here η is the normalized pressure gradient, which is given by

$$\eta = -\frac{1}{r \Omega_K^2} \frac{1}{\rho_g} \frac{\partial P}{\partial r}, \quad (20)$$

and $P = \rho_g c_s^2$ is the gas pressure at the midplane. We note that v_{drift} is not the radial velocity of dust particles toward the central star but the radial drift velocity relative to the gas (see Desch et al. 2017). The radial velocity of dust particles toward the central star is the sum of v_{adv} and v_{drift} .

2.2.2. Stokes number of dust particles

The Stokes number is the key parameter for the radial drift of dust particles and controls the velocities of dust particles. Assuming that fragmentation limits dust growth¹, the Stokes number of dust particles is given by the equilibrium between the mutual collision velocities and the fragmentation velocity:

$$\Delta v = v_{\text{frag}}, \quad (21)$$

where Δv is the mutual collision velocity, which depends on St , and v_{frag} is the threshold velocity for collisional fragmentation/growth. The mutual collision velocity is given by

$$(\Delta v)^2 = (\Delta v_r)^2 + (\Delta v_t)^2, \quad (22)$$

where Δv_r and Δv_t are the contributions from radial drift (e.g., Adachi et al. 1976) and gas turbulence (e.g., Ormel & Cuzzi 2007), respectively. For the case of $10^{-4} \lesssim St \ll 1$, Okuzumi et al. (2016) found that the radial drift term is given by

$$\Delta v_r \simeq 0.5 St \eta r \Omega_K, \quad (23)$$

and the gas turbulence term is given by

$$\Delta v_t \simeq \sqrt{2.3 \alpha_{\text{turb}} St c_s}, \quad (24)$$

where α_{turb} is the dimensionless parameter for the strength of turbulence. Then, we can calculate the Stokes number from Equation (22), which is the quadratic equation for St .

¹ We note that radial drift toward the central star may limit dust growth when the Stokes number exceeds $\sim 10^{-1}$, even if we do not consider fragmentation (e.g., Okuzumi et al. 2012; Okuzumi & Tazaki 2019).

The strength of turbulence should be associated with the strength of mass diffusion. Therefore, the two alpha parameters, α_{turb} and α_{acc} , might be related with the Schmidt number, which is the ratio of the kinematic viscosity to the mass diffusion coefficient. We simply assume the following equation:

$$\alpha_{\text{turb}} = \frac{\alpha_{\text{acc}}}{Sc}, \quad (25)$$

although we set $Sc = 1$ in the main part of this study otherwise noted. Hence, $\alpha_{\text{turb}} = \alpha_{\text{acc}}$ is assumed.

We assume that vertical settling of dust particles balances with turbulent diffusion. The dust scale height, h_d , and the midplane dust density, ρ_d , are given by Youdin & Lithwick (2007):

$$h_d = h_g \left(1 + \frac{St}{\alpha_{\text{turb}}} \frac{1 + 2St}{1 + St} \right)^{-1/2}, \quad (26)$$

$$\rho_d = \frac{\Sigma_{\text{dust}}}{\sqrt{2\pi} h_d}. \quad (27)$$

2.2.3. Conversion of dust to planetesimals

When the dust-to-gas mass ratio at the midplane is sufficiently high, hydrodynamic simulations revealed that part of pebbles would be converted into planetesimals via the streaming instability (e.g., Carrera et al. 2015; Yang et al. 2017; Sekiya & Onishi 2018)². Following the approach of Drazkowska et al. (2016), we take into account the effect of planetesimal formation. When the midplane dust density is higher than the gas density, $\rho_d > \rho_g$, we convert part of dust into planetesimals as follows (Drazkowska et al. 2016; Ueda et al. 2019):

$$\dot{\Sigma}_{\text{plts}} = \begin{cases} -\frac{\zeta}{2\pi} \Sigma_{\text{dust}} \Omega_K & (\rho_d > \rho_g), \\ 0 & (\rho_d \leq \rho_g), \end{cases} \quad (28)$$

where $\zeta = 10^{-4}$ is the planetesimal formation efficiency.

In this study, we consider two types of dust particles. As the mass loss rate of crystalline dust particles should be proportional to the crystallinity, the mass loss rate of dust particles via conversion of dust to planetesimal is given by

$$\dot{\Sigma}_{\text{plts},i} = -\frac{\zeta}{2\pi} \Sigma_i \Omega_K. \quad (29)$$

3. RESULTS

² We acknowledge that hydrodynamic simulations of planetesimal formation via the streaming instability usually assumed protoplanetary disks with negative pressure gradient (e.g., Bai & Stone 2010a,b; Carrera et al. 2015; Yang et al. 2017), and whether planetesimals can also be formed via the streaming instability in disks with positive pressure gradient is unclear. Although a high value of $\rho_d/\rho_g \gtrsim 1$ should be beneficial to make planetesimals via instabilities, further studies on the condition for planetesimal formation are needed.

In Section 3, we show the results of the disk evolution and radial distribution of the crystallinity of silicate dust particles. The results for disks without disk winds are shown in Section 3.1, and the results for evolving disks with disk winds are shown in Section 3.2.

3.1. Accretion disks without disk winds

We performed the evolution of protoplanetary disks that evolve without disk winds. Figure 1 shows the time evolution of the radial distribution of the crystallinity of silicate dust particles. We set $\alpha_{\text{acc}} = 10^{-3}$, $C_w = 0$, and $\text{Sc} = 1$ in Section 3.1, and we changed the value of v_{frag} as a parameter.

Figure 1(a) shows the radial distribution of the crystallinity for the case of $v_{\text{frag}} = 0 \text{ m s}^{-1}$ (i.e., $\text{St} = 0$). In this case, we found that the radial distribution at $t = 2 \text{ Myr}$ is approximately identical to that obtained from the analytic solution for steady-state accretion disks in $r \ll r_0$. Assuming that dust particles are dynamically coupled with gas (i.e., $\text{St} = 0$), Pavlyuchenkov & Dullemond (2007) derived that the radial distribution of the crystallinity in steady-state disks is given by

$$C = \begin{cases} 1 & (r \leq r_c), \\ \left(\frac{r}{r_c}\right)^{(3/2)\text{Sc}} & (r > r_c), \end{cases} \quad (30)$$

where $r_c = 1 \text{ au}$ is the location of the crystallization front. Here we assume that the background value of the crystallinity at $r = \infty$ is zero.

In contrast, the radial distribution of the crystallinity is different from the analytical solution when $v_{\text{frag}} \neq 0 \text{ m s}^{-1}$ (i.e., $\text{St} \neq 0$). Figures 1(b) and 1(c) show the radial distribution of the crystallinity for the cases of $v_{\text{frag}} = 1 \text{ m s}^{-1}$ and $v_{\text{frag}} = 3 \text{ m s}^{-1}$, respectively. We found that the crystallinity decreases with increasing v_{frag} . The radial distribution of the Stokes number at $t = 2 \text{ Myr}$ is shown in Figure 2. The Stokes number increases with r in most parts of the disk. This is because the mutual collision velocity is given by $\Delta v \simeq \Delta v_t$ and therefore $\sqrt{\text{St}c_s}$ is approximately constant (see Equations (21)–(24)).

The radial distribution of the crystalline silicate dust particles is given by the balance among three physical processes, that is, advection, radial drift, and diffusion of crystalline dust particles. We define the timescales of these processes as follows:

$$t_{\text{adv}} = \frac{r}{v_{\text{adv}}}, \quad (31)$$

$$t_{\text{drift}} = \frac{r}{v_{\text{drift}}}, \quad (32)$$

$$t_{\text{c,diff}} = \frac{r}{v_{\text{c,diff}}}. \quad (33)$$

Figure 3 shows the timescales of advection, radial drift, and diffusion at $t = 2 \text{ Myr}$. We found that the diffusion

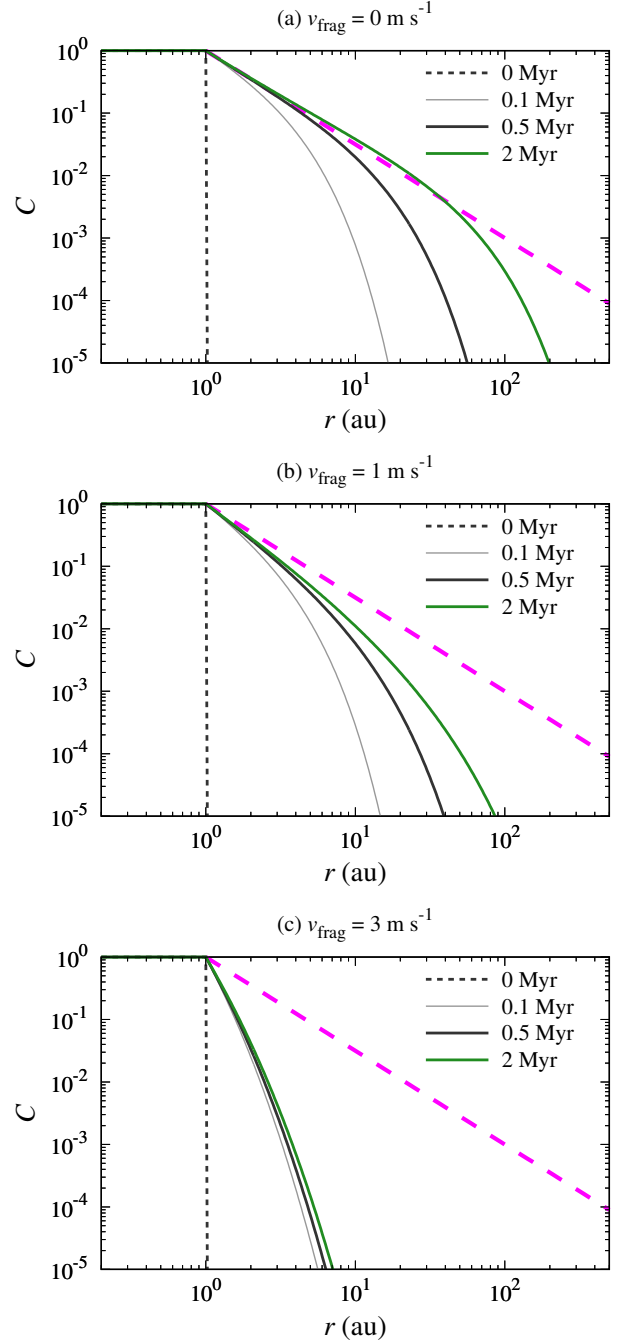


Figure 1. Radial distribution of the crystallinity. (a) For the case of $v_{\text{frag}} = 0 \text{ m s}^{-1}$ (i.e., $\text{St} = 0$). (b) For the case of $v_{\text{frag}} = 1 \text{ m s}^{-1}$. (c) For the case of $v_{\text{frag}} = 3 \text{ m s}^{-1}$. We set $\alpha_{\text{acc}} = 10^{-3}$, $C_w = 0$, and $\text{Sc} = 1$. The magenta dashed line shows the analytical solution of the radial distribution of the crystallinity in steady state disks (Equation 30).

timescale is negative in the region beyond the crystallization front ($r > r_c$). Therefore, the direction of the diffusion is outward. The diffusion timescale is balanced with the advection or radial drift timescales. In particular, the radial drift

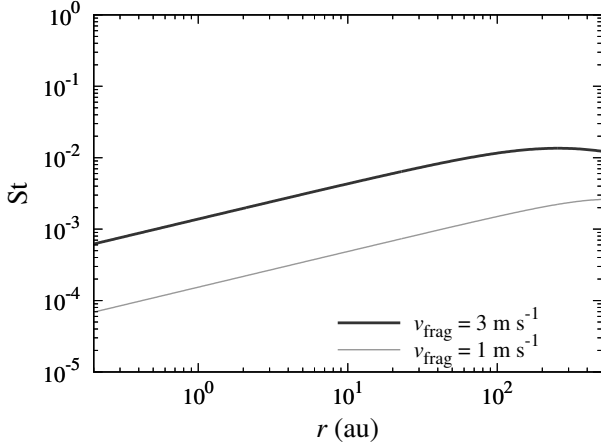


Figure 2. Radial distribution of the Stokes number at $t = 2$ Myr. We set $\alpha_{\text{acc}} = 10^{-3}$, $C_w = 0$, and $Sc = 1$.

and diffusion timescales are balanced when the radial drift timescale is shorter than the advection timescale (see Figure 3(c)).

For the case of $v_{\text{frag}} = 0 \text{ m s}^{-1}$, crystalline dust particles do not drift relative to the gas but diffuse due to the gradient of $\Sigma_c/\Sigma_{\text{gas}}$. The equilibrium of the radial distribution of the crystallinity is given by the balance between diffusion and advection. The radial distribution of the crystallinity at $t = 2$ Myr is approximately consistent with the steady-state solution (Equation 30) at $r \ll r_0$.

In contrast, for the case of $v_{\text{frag}} = 3 \text{ m s}^{-1}$, crystalline dust particles drift inwardly, and the effect of the inward advection is negligibly smaller than that of radial drift (Figure 3(c)). The equilibrium of the radial distribution of the crystallinity is given by the balance between diffusion and strong radial drift. Thus, outward transport of crystalline dust particles are suppressed compared to the case of $v_{\text{frag}} = 0 \text{ m s}^{-1}$. Figure 1(c) shows that the radial distribution of the crystallinity already reaches the steady state at $t = 2$ Myr. As the radial drift timescale is inversely proportional to the Stokes number, calculations with a large value of v_{frag} lead to the depletion of the crystallinity beyond the crystallization front for the case of disks that evolve without disk winds. This result is qualitatively inconsistent with the observed findings that crystalline dust particles are found farther away from the crystallization front.

3.2. Evolving disks due to disk winds

We performed the evolution of protoplanetary disks that evolve due to disk winds. Figure 4 shows the radial distributions of the gas pressure at the midplane and the gas surface density. We set $\alpha_{\text{acc}} = 10^{-4}$, $C_w = 10^{-5}$, and $Sc = 1$ in Section 3.2.

Figure 4(a) shows the evolution of the radial distributions of the gas pressure at the midplane. As shown in previous

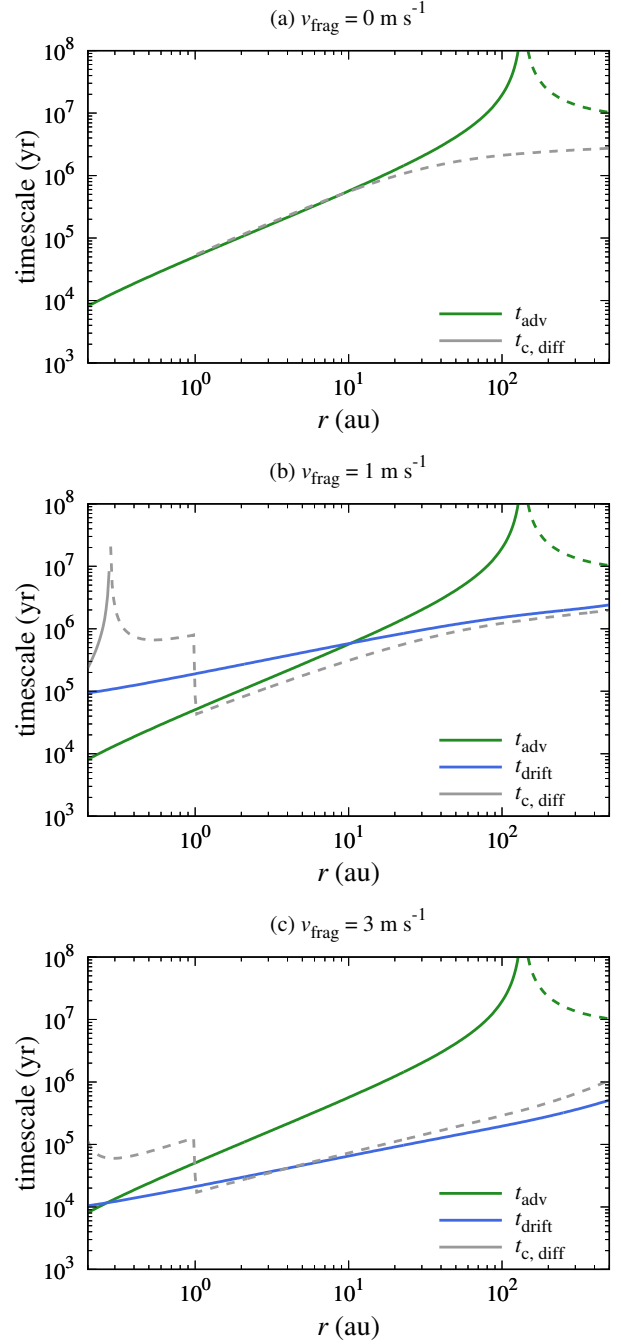


Figure 3. Timescales of advection, radial drift, and diffusion at $t = 2$ Myr. (a) For the case of $v_{\text{frag}} = 0 \text{ m s}^{-1}$. (b) For the case of $v_{\text{frag}} = 1 \text{ m s}^{-1}$. (c) For the case of $v_{\text{frag}} = 3 \text{ m s}^{-1}$. We set $\alpha_{\text{acc}} = 10^{-3}$, $C_w = 0$, and $Sc = 1$. Solid lines indicate that the timescales are positive, i.e., the direction of the flows is inward, and dashed lines indicate that the timescales are negative.

studies (e.g., Suzuki et al. 2016; Takahashi & Muto 2018), magnetically driven disk winds creates a maximum of gas pressure. Takahashi & Muto (2018) revealed that the location of the pressure maximum moves outward with time because

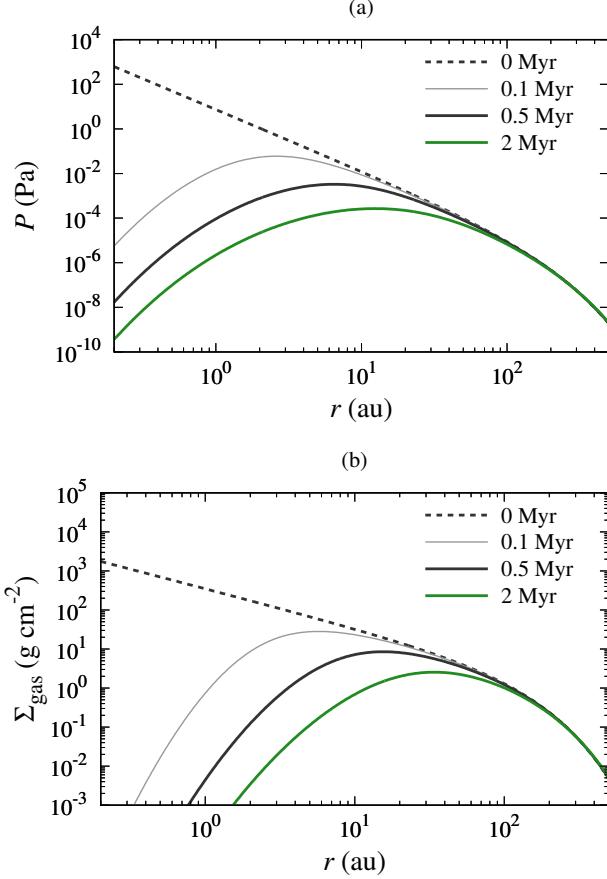


Figure 4. Radial distributions of (a) the gas pressure at the midplane and (b) the gas surface density. We set $\alpha_{\text{acc}} = 10^{-4}$, $C_w = 10^{-5}$, and $\text{Sc} = 1$.

the timescale of wind mass loss is longer for a larger orbital radius. Our result is consistent with that of [Takahashi & Muto \(2018\)](#). The location of the pressure maximum at $t = 2$ Myr is $r = 12$ au, and this is approximately consistent with that obtained from the analytical solution for steady-state disks with viscous accretion and magnetically driven disk winds (see Appendix A).

Figure 4(b) also shows the evolution of the gas surface density. It is clear that the locations of the maxima of the gas pressure and gas surface density are different: the location of the pressure maximum is inner than that of the gas surface density. This relation is also explained by the analytical solution for steady-state disks (see Appendix A).

Figure 5(a) shows the radial distribution of the dust surface density for the case of $v_{\text{frag}} = 3 \text{ m s}^{-1}$. We found that a narrow dust ring is formed in the disk, and the location is approximately identical to that of the pressure maximum. This is because large pebbles are accumulated around the pressure maximum (e.g., [Haghighipour & Boss 2003](#); [Takahashi & Muto 2018](#)). The dust surface density is significantly depleted beyond the dust ring due to the inward radial drift of

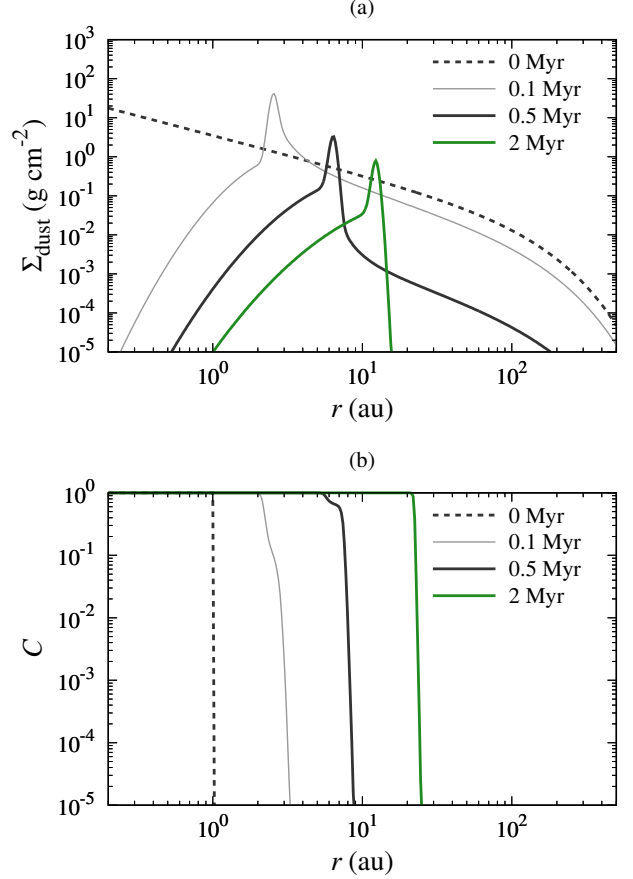


Figure 5. Radial distribution of (a) the dust surface density and (b) the crystallinity of silicate dust particles with $v_{\text{frag}} = 3 \text{ m s}^{-1}$. We set $\alpha_{\text{acc}} = 10^{-4}$, $C_w = 10^{-5}$, and $\text{Sc} = 1$.

large pebbles. Inside the dust ring, the dust surface density is controlled by the conversion of dust to planetesimals (see Section 2.2.3). Figure 6 shows the radial distribution of the dust-to-gas mass ratio. We found that the dust surface density inside the dust ring is approximately given by the following equation: $\rho_d = \rho_g$. This is because the conversion of dust particles to planetesimals occurs immediately when $\rho_d > \rho_g$ (see Equation 28).

The radial distribution of the Stokes number at $t = 2$ Myr is shown in Figure 7. We set $\alpha_{\text{acc}} = 10^{-4}$ instead of $\alpha_{\text{acc}} = 10^{-3}$ in Section 3.2, and the Stokes number shown in Figure 7 is larger than that shown in Figure 2. For the case of $v_{\text{frag}} = 3 \text{ m s}^{-1}$, the Stokes number is in the range of $10^{-2} \lesssim \text{St} \lesssim 10^{-1}$ throughout the disk. This Stokes number provides the values of the dust-to-gas mass ratio under $\rho_d = \rho_g$. The dust scale height is given by Equation (26), and the midplane dust density is inversely proportional to the dust scale height.

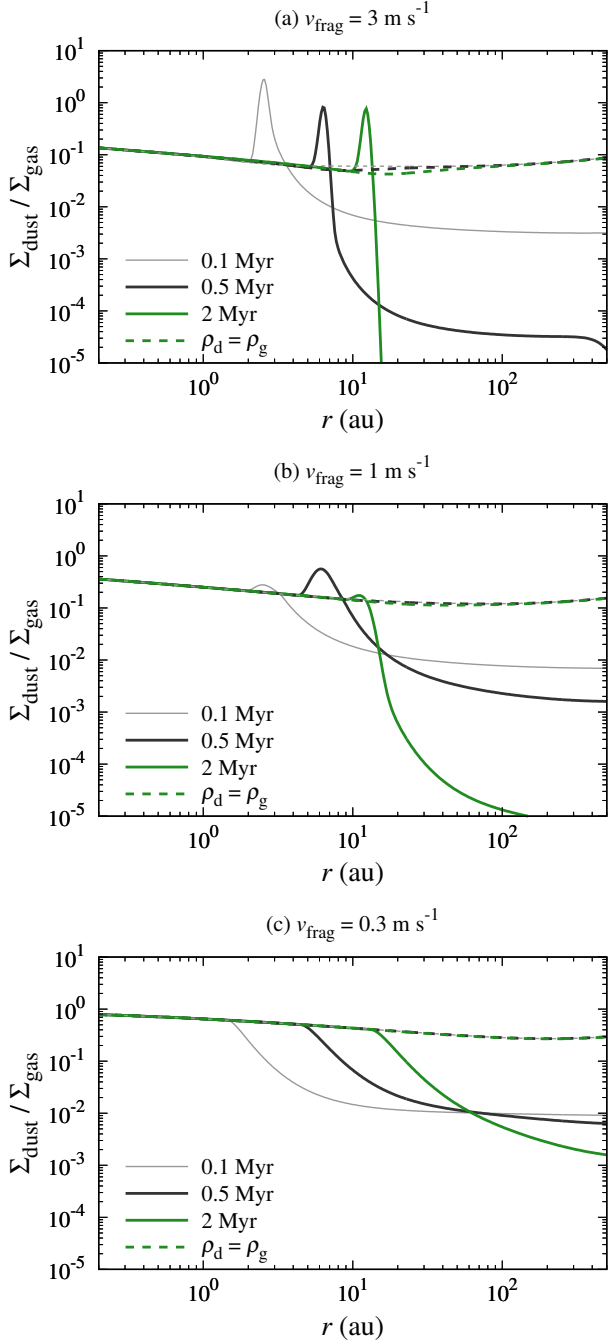


Figure 6. Radial distribution of the dust-to-gas mass ratio, $\Sigma_{\text{dust}}/\Sigma_{\text{gas}}$. (a) For the case of $v_{\text{frag}} = 3 \text{ m s}^{-1}$. (b) For the case of $v_{\text{frag}} = 1 \text{ m s}^{-1}$. (c) For the case of $v_{\text{frag}} = 0.3 \text{ m s}^{-1}$. We set $\alpha_{\text{acc}} = 10^{-4}$, $C_w = 10^{-5}$, and $\text{Sc} = 1$. Dashed lines show the analytical estimates from Equation (34).

Therefore, $\Sigma_{\text{dust}}/\Sigma_{\text{gas}}$ is given by

$$\frac{\Sigma_{\text{dust}}}{\Sigma_{\text{gas}}} = \left(1 + \frac{\text{St}}{\alpha_{\text{turb}}} \frac{1 + 2\text{St}}{1 + \text{St}} \right)^{-1/2}, \quad (34)$$

$$\simeq \sqrt{\frac{\alpha_{\text{turb}}}{\text{St}}}, \quad (35)$$

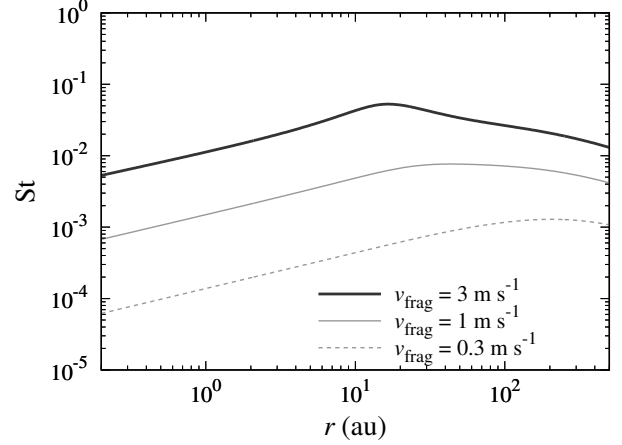


Figure 7. Radial distribution of the Stokes number at $t = 2 \text{ Myr}$.

when $\rho_d = \rho_g$ is achieved. This estimation explains the radial distribution of $\Sigma_{\text{dust}}/\Sigma_{\text{gas}}$ shown in Figure 6.

Figure 5(b) shows the radial distribution of the crystallinity of silicate dust particles for the case of $v_{\text{frag}} = 3 \text{ m s}^{-1}$. We found that the crystallinity is almost 100% around and inside the location of the dust ring. The radial distribution of the crystallinity shown in Figure 5(b) is completely different from that for disks without disk winds. In Section 3.3, we unveil the mechanism for the radial transport of crystalline dust particles in evolving disk due to disk wind. The key physics of the efficient radial transport is the *outward radial drift* of pebbles.

Figures 8 and 9 show the radial distributions of Σ_{dust} and C for the cases of $v_{\text{frag}} = 1 \text{ m s}^{-1}$ and $v_{\text{frag}} = 0.3 \text{ m s}^{-1}$, respectively. As shown in Figure 8(a), the radial distribution of the dust surface density for the case of $v_{\text{frag}} = 1 \text{ m s}^{-1}$ is similar to that for the case of $v_{\text{frag}} = 3 \text{ m s}^{-1}$, although the width and the maximum value of Σ_{dust} of the dust ring are different. The radial distribution of the crystallinity shown in Figure 8(b) is also similar to that shown in Figure 5(b).

In contrast, the radial distributions of Σ_{dust} and C for the cases of $v_{\text{frag}} = 0.3 \text{ m s}^{-1}$ are completely different from those for $v_{\text{frag}} = 3 \text{ m s}^{-1}$. As shown in Figure 9(a), the dust surface density hardly changes with time beyond the maximum of the dust surface density. On the other hand, inside the maximum of the dust surface density, the dust-to-gas mass ratio is controlled by Equation (34). Then, the dust surface density is approximately given by the following equation for the case of small pebbles: $\Sigma_{\text{dust}} \simeq \min\left(\sqrt{\alpha_{\text{turb}}/\text{St}}\Sigma_{\text{gas}}, \Sigma_{\text{dust},0}\right)$. The location of the dust ring is therefore not necessarily identical to that of the pressure maximum.

The radial distribution of the crystallinity of silicate dust particles with $v_{\text{frag}} = 0.3 \text{ m s}^{-1}$ is shown in Figure 9(b). In contrast to the radial distribution shown in Figures 5(b) and 8(b), the crystallinity is $C < 1$ outside the crystallization

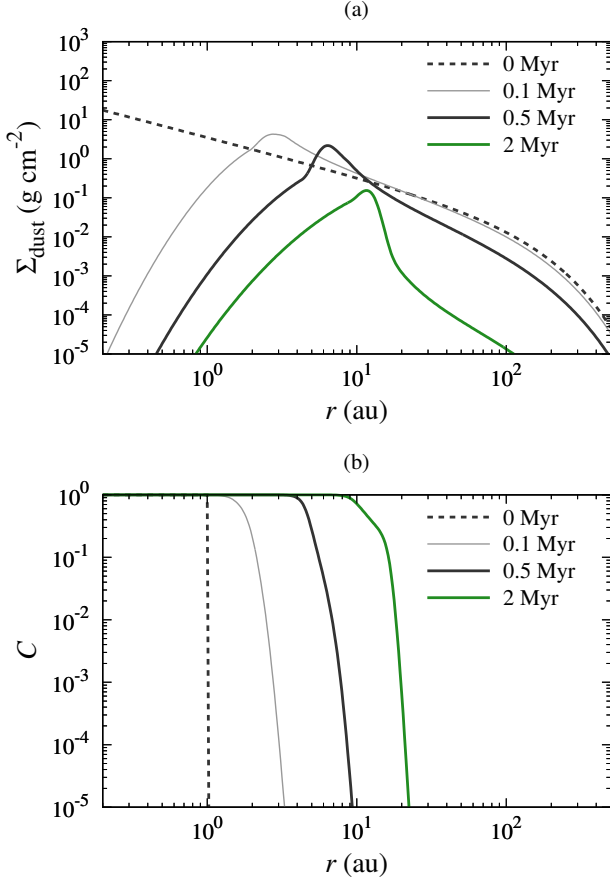


Figure 8. Radial distribution of (a) the dust surface density and (b) the crystallinity of silicate dust particles with $v_{\text{frag}} = 1 \text{ m s}^{-1}$. We set $\alpha_{\text{acc}} = 10^{-4}$, $C_w = 10^{-5}$, and $\text{Sc} = 1$.

front, and the crystallinity decreases with increasing r . The crystallinity around the dust ring is $C \ll 1$ for the case of $v_{\text{frag}} = 0.3 \text{ m s}^{-1}$.

3.3. Outward radial drift as a new mechanism for radial transport of crystalline dust particles

As shown in Figures 5(b) and 8(b), the crystallinity is almost 100% around and inside the location of the dust ring when the threshold velocity for collisional fragmentation/growth is $v_{\text{frag}} \geq 1 \text{ m s}^{-1}$. In Section 3.3, we show the condition for driving efficient radial transport.

Figure 10 shows the timescales of advection, radial drift, and diffusion at $t = 2 \text{ Myr}$. Inside the pressure maximum, the radial drift timescale is negative while the advection timescale is positive. For the case of $v_{\text{frag}} \geq 1 \text{ m s}^{-1}$, the Stokes number of pebbles is large and the radial drift timescale is shorter than the advection timescale: $|t_{\text{drift}}| < |t_{\text{adv}}|$ (see Figures 10(a) and 10(b)). In this case, the outward radial drift of pebbles can transport the crystalline dust particles from the crystallization front to the pressure max-

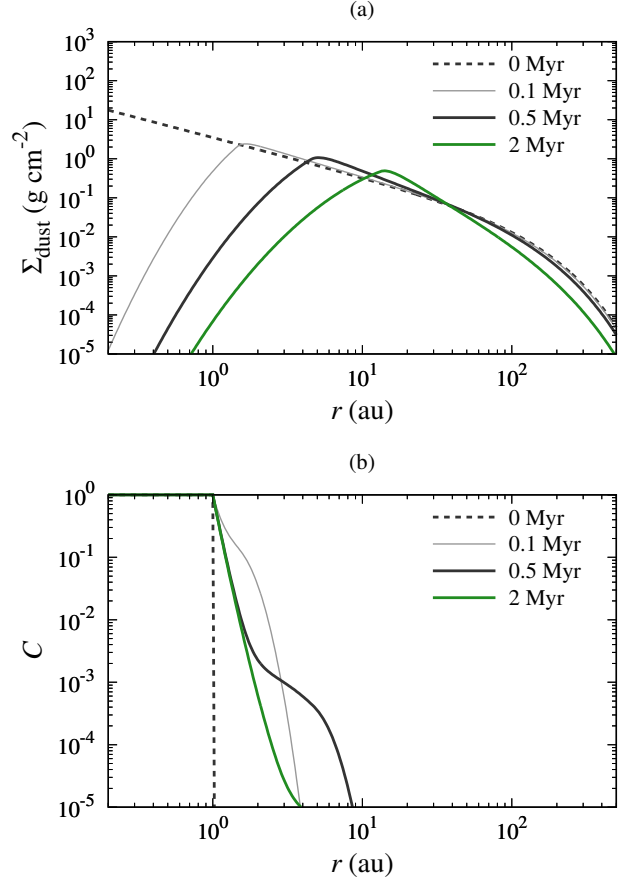


Figure 9. Radial distribution of (a) the dust surface density and (b) the crystallinity of silicate dust particles with $v_{\text{frag}} = 0.3 \text{ m s}^{-1}$. We set $\alpha_{\text{acc}} = 10^{-4}$, $C_w = 10^{-5}$, and $\text{Sc} = 1$.

imum. Then, the crystallinity reaches almost 100% around and inside the location of the dust ring.

In contrast, for the case of $v_{\text{frag}} = 0.3 \text{ m s}^{-1}$, the Stokes number of pebbles is small and the radial drift timescale is longer than the advection timescale: $|t_{\text{drift}}| > |t_{\text{adv}}|$ (see Figure 10(c)). In this case, the outward radial drift of pebbles *cannot* transport the crystalline dust particles efficiently. Then, the diffusion timescale is balanced with the advection timescale, and the crystallinity decreases with increasing r .

Our novel mechanism for the radial transport of crystalline dust particles is illustrated in Figure 11. The condition for driving efficient radial transport by the outward radial drift is $|t_{\text{drift}}| < |t_{\text{adv}}|$. As the radial drift timescale is inversely proportional to the Stokes number, calculations with a large value of v_{frag} lead to the efficient radial transport. Therefore, we expect that the crystallinity around and inside the dust ring reflects the size of pebbles and the threshold velocity for collisional fragmentation/growth.

By comparing our calculations with the observational findings that the crystalline silicate dust particles exist in the cold regions of the protoplanetary disks and the solar nebula, we

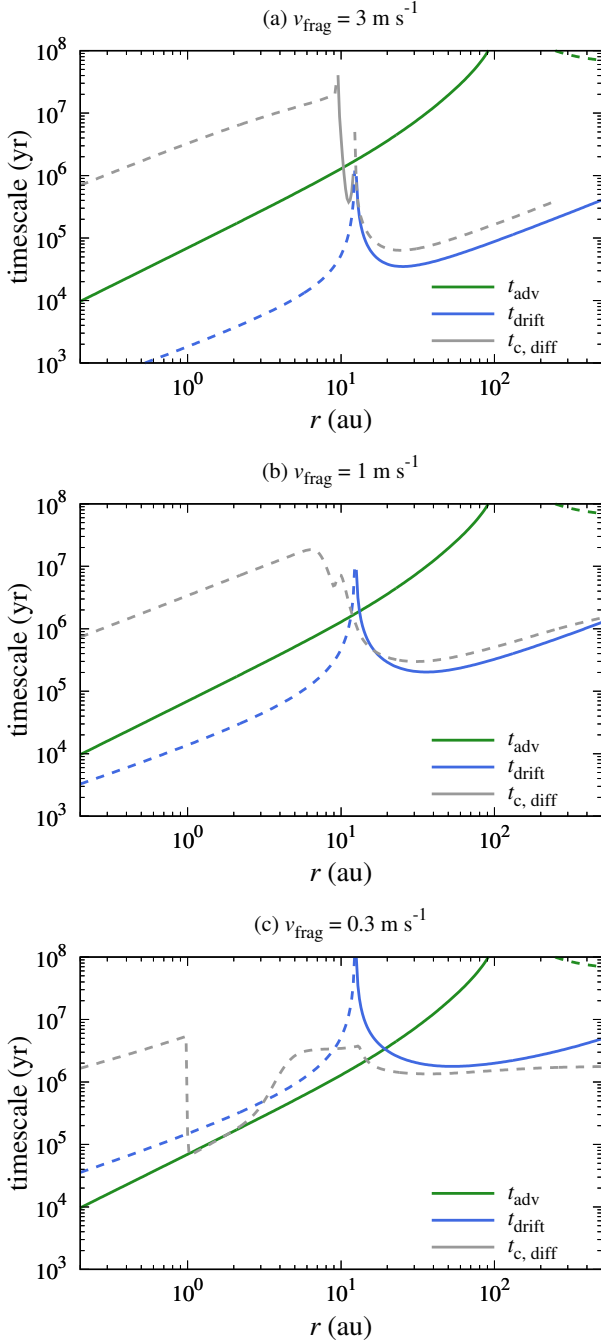


Figure 10. Timescales of advection, radial drift, and diffusion at $t = 2$ Myr. (a) For the case of $v_{\text{frag}} = 3 \text{ m s}^{-1}$. (b) For the case of $v_{\text{frag}} = 1 \text{ m s}^{-1}$. (c) For the case of $v_{\text{frag}} = 0.3 \text{ m s}^{-1}$. We set $\alpha_{\text{acc}} = 10^{-4}$, $C_w = 10^{-5}$, and $\text{Sc} = 1$.

suggest that this outward radial drift would be the key mechanism to transport crystalline silicate dust particles. This idea is supported by the fact that the recent high-spatial-resolution observations revealed that the ring structures are relatively common among protoplanetary disks. As the radial structures of gas disks strongly affect the dynamics of pebbles,

further observational studies on the link between disk structure and dust composition are required.

4. DEPENDENCE ON THE SCHMIDT NUMBER

In Section 3, we set $\text{Sc} = 1$ for simplicity. However, the Schmidt number of protoplanetary disks does not necessarily have to be $\text{Sc} = 1$. Three-dimensional magneto-hydrodynamic simulations indicated that the turbulent diffusion due to magneto-rotational instability is expressed by the Schmidt number with $0.85 \lesssim \text{Sc} \lesssim 10$ (Carballido et al. 2005; Johansen & Klahr 2005). Based on analytic arguments, Pavlyuchenkov & Dullemond (2007) also derived the theoretical minimum value of $\text{Sc} = 1/3$. In Section 4, we briefly review the dependence of the radial distribution of the crystalline dust particles on the Schmidt number.

4.1. Accretion disks without disk winds

Here we show the results for accretion disks without disk winds in Section 4.1. Figure 12 shows the time evolution of the radial distribution of the crystallinity of silicate dust particles. Here we set $\alpha_{\text{acc}} = 10^{-3}$, $C_w = 0$, and $v_{\text{frag}} = 0 \text{ m s}^{-1}$, and we changed the value of Sc as a parameter.

We confirmed that the radial distribution at $t = 2$ Myr is approximately identical to that obtained from the analytical solution for steady-state accretion disks: $C = (r/r_c)^{(3/2)\text{Sc}}$ (Pavlyuchenkov & Dullemond 2007). Therefore, the radial distribution of the crystallinity is a sensitive function of Sc for the case of classical accretion disks without disk winds as shown in previous studies (e.g., Clarke & Pringle 1988; Pavlyuchenkov & Dullemond 2007). It should be noted that these radial distributions of the crystallinity are derived under $v_{\text{frag}} = 0 \text{ m s}^{-1}$. The radial distribution of the crystallinity is determined by the balance among the advection, diffusion, and radial drift when $v_{\text{frag}} \neq 0 \text{ m s}^{-1}$ (Section 3.1).

4.2. Evolving disks due to disk winds

In contrast, the radial distribution of the crystallinity is *not* a sensitive function of Sc for the case of evolving disks due to disk winds. We set $\alpha_{\text{acc}} = 10^{-4}$, $C_w = 10^{-5}$, $v_{\text{frag}} = 1 \text{ m s}^{-1}$, and $\text{Sc} = 2$ in Section 4.2. Figure 13(a) shows the radial distribution of the dust surface density. A dust ring is formed around the pressure maximum as in the case of Figures 5(a) and 8(a). Figure 13(b) shows the radial distribution of the crystallinity of silicate dust particles. The crystallinity is almost 100% around and inside the location of the dust ring as in the case of Figures 5(b) and 8(b).

Figure 14 shows the timescales of advection, radial drift, and diffusion at $t = 2$ Myr. In this case, the Stokes number of pebbles is large enough to satisfy the following condition: $|t_{\text{drift}}| < |t_{\text{adv}}|$. Then, the outward radial drift of pebbles can transport the crystalline dust particles from the crystallization front to the pressure maximum, and the crystallinity reaches almost 100% around and inside the location of the dust ring.

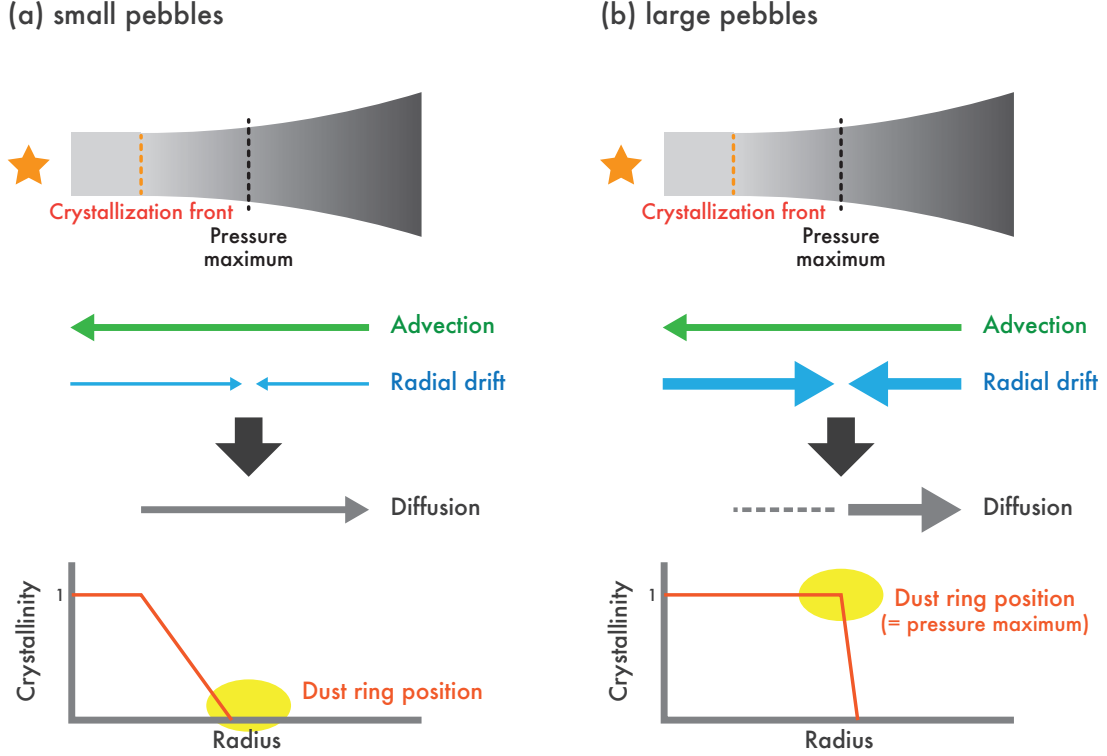


Figure 11. Schematic of the radial transport processes in evolving protoplanetary disks due to magnetically driven disk winds. (a) For the case of small pebbles, i.e., $|t_{\text{drift}}| > |t_{\text{adv}}|$. The outward radial drift of pebbles cannot transport the crystalline dust particles, and the diffusion timescale is balanced with the advection timescale. (b) For the case of large pebbles, i.e., $|t_{\text{drift}}| < |t_{\text{adv}}|$. If the radial drift timescale is shorter than the advection timescale, the *outward radial drift* of pebbles can transport the crystalline dust particles from the crystallization front to the pressure maximum efficiently.

For the case of classical accretion disks without disk winds, the radial distribution of the crystallinity is given by the balance of the diffusion and advection (or radial drift) timescales. In contrast, for the case of evolving disks due to disk winds, the radial distribution of the crystallinity is almost 100% if the outward radial drift overcomes the inward advection. As the diffusion is not the main mechanism, the radial distribution of the crystallinity hardly depends on Sc as long as the condition for the outward radial drift (i.e., $|t_{\text{drift}}| < |t_{\text{adv}}|$) is satisfied (see Figure 11).

5. SUMMARY

Several pieces of evidence suggest that silicate dust particles undergo significant thermal processing in protoplanetary disks, and crystalline dust particles should transport outwardly as they are found in the outer region of protoplanetary disks and the solar system. Several mechanisms have been proposed for the outward transport of crystalline dust particles (e.g., Gail 2001; Keller & Gail 2004; Dullemond et al. 2006; Ciesla 2010; Yang & Ciesla 2012).

Recent astronomical observations revealed varieties of structures of protoplanetary disks. In particular, the dust ring structures are observed in a large number of disks, and the accumulation of pebbles around the pressure maximum cre-

ated by mass loss due to magnetically driven disk winds is one of the possible origins of the observed dust ring structure (e.g., Takahashi & Muto 2018).

In this study, we proposed a novel mechanism for the outward transport of crystalline dust particles. In evolving protoplanetary disks due to magnetically driven disk winds, dust particles can migrate outwardly by radial drift. We found that the outward radial drift process can transport crystalline dust particles efficiently when the radial drift overcomes the advective flow. Our findings are summarized as follows.

1. In Section 3.1, we performed the evolution of protoplanetary disks that evolve without disk winds. The diffusion timescale is balanced with the advection or inward radial drift timescales (see Figure 3); the crystallinity is well expressed by the analytical estimation by Pavlyuchenkov & Dullemond (2007) when the advection balances with the diffusion. It should be noted that the inward radial drift significantly suppresses the outward transport of the crystalline dust particles, which is inconsistent with the observational evidence.
2. In Section 3.2, we performed the evolution of protoplanetary disks that evolve due to disk winds. As shown in previous studies (e.g., Suzuki et al. 2016;

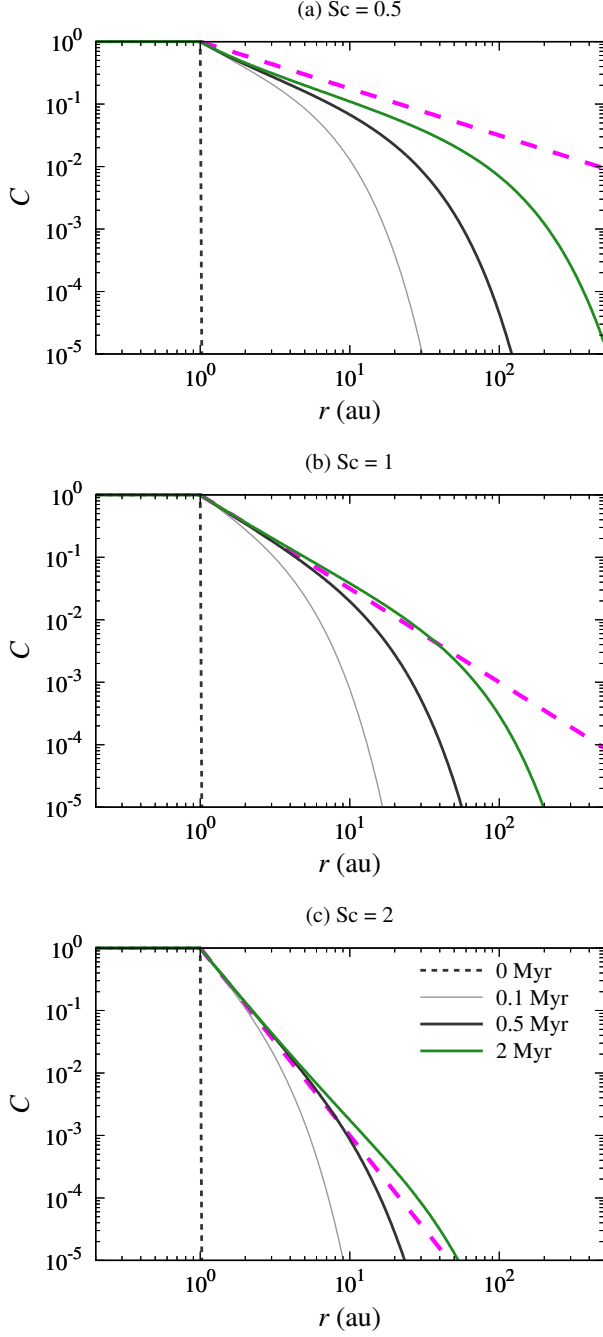


Figure 12. Radial distribution of the crystallinity. (a) For the case of $Sc = 0.5$. (b) For the case of $Sc = 1$. (c) For the case of $Sc = 2$. We set $\alpha_{\text{acc}} = 10^{-3}$, $C_w = 0$, and $v_{\text{frag}} = 0 \text{ m s}^{-1}$. The magenta dashed line shows the analytical solution of the radial distribution of the crystallinity in steady state disks (Equation 30).

(Takahashi & Muto 2018), magnetically driven disk winds create a maximum of gas pressure at a certain radius (see Figure 4). We found that the location of the pressure maximum at $t = 2 \text{ Myr}$ is approximately consistent with that obtained from the analytical solu-

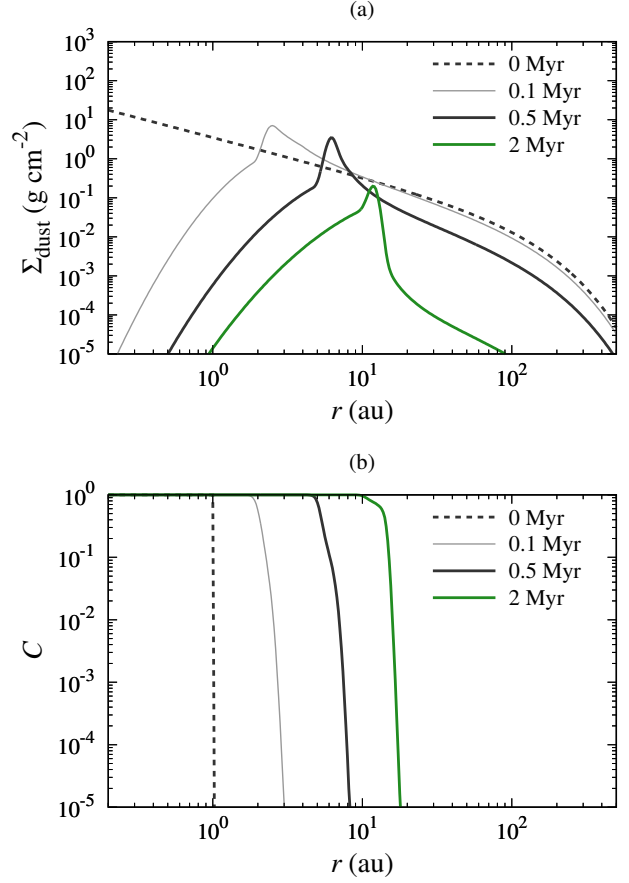


Figure 13. Radial distribution of (a) the dust surface density and (b) the crystallinity of silicate dust particles. We set $\alpha_{\text{acc}} = 10^{-4}$, $C_w = 10^{-5}$, $v_{\text{frag}} = 1 \text{ m s}^{-1}$, and $Sc = 2$.

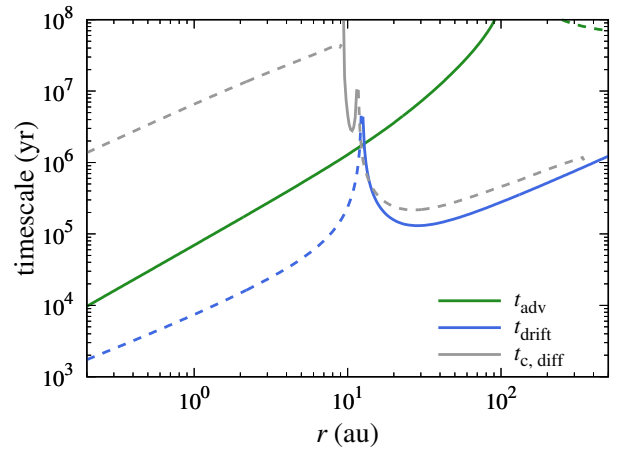


Figure 14. Timescales of advection, radial drift, and diffusion at $t = 2 \text{ Myr}$. We set $\alpha_{\text{acc}} = 10^{-4}$, $C_w = 10^{-5}$, $v_{\text{frag}} = 1 \text{ m s}^{-1}$, and $Sc = 2$.

tion for steady-state disks with viscous accretion and magnetically driven disk winds (see Appendix A).

3. Figure 5(a) shows the radial distribution of the dust surface density. For the case of $v_{\text{frag}} = 3 \text{ m s}^{-1}$, a narrow dust ring is formed in the disk, and the location is approximately identical to that of the pressure maximum. This is because large pebbles are accumulated around the pressure maximum (e.g., Haghighipour & Boss 2003; Takahashi & Muto 2018).
4. Figure 5(b) shows the radial distribution of the crystallinity of silicate dust particles. For the case of $v_{\text{frag}} = 3 \text{ m s}^{-1}$, the crystallinity is almost 100% around and inside the location of the dust ring. We proposed that the key physics of the efficient outward radial transport is the outward radial drift of pebbles.

5. The mechanism for the radial transport of crystalline dust particles proposed in this study is illustrated in Figure 11. The condition for driving efficient radial transport by the outward radial drift is $|t_{\text{drift}}| < |t_{\text{adv}}|$. As the radial drift timescale is inversely proportional to the Stokes number, calculations with a large value of v_{frag} lead to the efficient radial transport. Therefore, we expect that the crystallinity around and inside the dust ring reflects the size of pebbles and the threshold velocity for collisional fragmentation/growth.

ACKNOWLEDGMENTS

We thank Shoji Mori, Taishi Nakamoto, and Tetsuo Taki for useful discussions. S.A. was supported by JSPS KAKENHI Grant No. JP20J00598. This work was supported by the Publications Committee of NAOJ.

APPENDIX

A. STATIONARY SOLUTION FOR GAS DISK

We found a stationary solution for the gas surface density of disk with viscous accretion and magnetically driven disk winds. We set the radial distribution of the midplane temperature and the sound velocity as follows:

$$T = T_1 \tilde{r}^{-q}, \quad (\text{A1})$$

$$c_s = c_{s,1} \tilde{r}^{-q/2}, \quad (\text{A2})$$

where $\tilde{r} \equiv r/(1 \text{ au})$ is the normalized distance from the central star, and $c_{s,1} = (k_B T_1 / m_g)^{1/2}$ is the sound speed at $r = 1 \text{ au}$. Here k_B is the Boltzmann constant, and $m_g = 2.34 m_H$ is the mean molecular mass, where m_H is the mass of a hydrogen atom.

Assuming that a gas disk is in steady state, the left-hand side of Equation (3) is zero:

$$0 = \frac{1}{2\pi r} \frac{\partial \dot{M}_{\text{gas}}}{\partial r} - C_w \Sigma_{\text{gas}} \Omega_K. \quad (\text{A3})$$

We can rewrite the above equation as follows:

$$\begin{aligned} \tilde{r}^{3-q} \frac{\partial^2 \Sigma_{\text{gas}}}{\partial \tilde{r}^2} + \left(\frac{9}{2} - 2q \right) \tilde{r}^{2-q} \frac{\partial \Sigma_{\text{gas}}}{\partial \tilde{r}} \\ + \left[(2-q) \left(\frac{3}{2} - q \right) \tilde{r}^{1-q} - \mathcal{A} \right] \Sigma_{\text{gas}} = 0, \end{aligned} \quad (\text{A4})$$

where the dimensionless parameter \mathcal{A} is

$$\begin{aligned} \mathcal{A} &= \frac{C_w v_{K,1}^2}{3\alpha_{\text{acc}} c_{s,1}^2} \\ &= 26.1 \left(\frac{C_w / \alpha_{\text{acc}}}{10^{-1}} \right) \left(\frac{T_1}{800 \text{ K}} \right)^{-1} \left(\frac{M_\star}{2.5 M_\odot} \right), \end{aligned} \quad (\text{A5})$$

where $v_{K,1} = \sqrt{GM_\star / (1 \text{ au})}$ is the Kepler velocity at $r = 1 \text{ au}$.

We found that the solution of Equation (A4) is given as follows:

$$\Sigma_{\text{gas}} = \Sigma_0 \tilde{r}^{q-7/4} \frac{2(2p\mathcal{A}^{1/2})^p}{\Gamma(p)} K_p \left(4p\mathcal{A}^{1/2} \tilde{r}^{-1/(4p)} \right), \quad (\text{A6})$$

where $K_p(x)$ is the modified Bessel function of the second kind, and the exponent, p , is given by

$$p \equiv \frac{1}{2(1-q)}. \quad (\text{A7})$$

For the special case of $q = 1/2$ and $p = 1$, the stationary solution of Σ_{gas} for a gas disk with radial mass accretion and wind-driven mass loss is given by

$$\Sigma_{\text{gas}} = \Sigma_0 \tilde{r}^{-5/4} \cdot 4\mathcal{A}^{1/2} K_1 \left(4\mathcal{A}^{1/2} \tilde{r}^{-1/4} \right), \quad (\text{A8})$$

where Σ_0 is a parameter. In this case, Σ_{gas} takes the maximum at

$$r = 0.66 \mathcal{A}^2 \text{ au}. \quad (\text{A9})$$

We can also calculate the radial profile of the gas pressure at the midplane. The gas pressure is given by

$$\begin{aligned} P &= \frac{\Sigma_{\text{gas}} c_s \Omega_K}{\sqrt{2\pi}} \\ &= P_0 \tilde{r}^{q/2-13/4} \frac{2(2p\mathcal{A}^{1/2})^p}{\Gamma(p)} K_p \left(4p\mathcal{A}^{1/2} \tilde{r}^{-1/(4p)} \right), \end{aligned} \quad (\text{A10})$$

where P_0 is a constant. For the case of $q = 1/2$ and $p = 1$, we obtain the following equation:

$$P = P_0 \tilde{r}^{-3} \cdot 4\mathcal{A}^{1/2} K_1 \left(4\mathcal{A}^{1/2} \tilde{r}^{-1/4} \right). \quad (\text{A11})$$

In this case, P takes the maximum at

$$r = 0.015\mathcal{A}^2 \text{ au.} \quad (\text{A12})$$

Assuming $\mathcal{A} = 26.1$ (see Equation A5), the location of the pressure maximum in the steady-state disk is estimated to be $r = 10.1$ au. Our numerical simulation shows good agreement with this analytical prediction; the location of the

pressure maximum is around $r \simeq 12$ au at $t = 2$ Myr (see Figure 4). Thus the structure of the gas disk would already approach the steady-state solution at $t = 2$ Myr. We note, however, that the location of the maximum for the gas density is not consistent with the analytical prediction. This is because an exponential cutoff for the outer edge of the gas disk exists at $r \simeq 100$ au in our numerical simulation (see Equation 1), which is not taken into account in the analytic model for the steady-state disk.

REFERENCES

- Adachi, I., Hayashi, C., & Nakazawa, K. 1976, *Progress of Theoretical Physics*, 56, 1756, doi: [10.1143/PTP.56.1756](https://doi.org/10.1143/PTP.56.1756)
- ALMA Partnership, Brogan, C. L., Pérez, L. M., et al. 2015, *ApJL*, 808, L3, doi: [10.1088/2041-8205/808/1/L3](https://doi.org/10.1088/2041-8205/808/1/L3)
- Andrews, S. M. 2020, *ARA&A*, 58, 483, doi: [10.1146/annurev-astro-031220-010302](https://doi.org/10.1146/annurev-astro-031220-010302)
- Andrews, S. M., Huang, J., Pérez, L. M., et al. 2018, *ApJL*, 869, L41, doi: [10.3847/2041-8213/aaf741](https://doi.org/10.3847/2041-8213/aaf741)
- Bai, X.-N., & Stone, J. M. 2010a, *ApJL*, 722, L220, doi: [10.1088/2041-8205/722/2/L220](https://doi.org/10.1088/2041-8205/722/2/L220)
- . 2010b, *ApJ*, 722, 1437, doi: [10.1088/0004-637X/722/2/1437](https://doi.org/10.1088/0004-637X/722/2/1437)
- Boss, A. P. 2008, *Earth and Planetary Science Letters*, 268, 102, doi: [10.1016/j.epsl.2008.01.008](https://doi.org/10.1016/j.epsl.2008.01.008)
- Carballido, A., Stone, J. M., & Pringle, J. E. 2005, *MNRAS*, 358, 1055, doi: [10.1111/j.1365-2966.2005.08850.x](https://doi.org/10.1111/j.1365-2966.2005.08850.x)
- Carrera, D., Johansen, A., & Davies, M. B. 2015, *A&A*, 579, A43, doi: [10.1051/0004-6361/201425120](https://doi.org/10.1051/0004-6361/201425120)
- Ciesla, F. J. 2007, *Science*, 318, 613, doi: [10.1126/science.1147273](https://doi.org/10.1126/science.1147273)
- . 2009, *Icarus*, 200, 655, doi: [10.1016/j.icarus.2008.12.009](https://doi.org/10.1016/j.icarus.2008.12.009)
- . 2010, *Icarus*, 208, 455, doi: [10.1016/j.icarus.2010.02.010](https://doi.org/10.1016/j.icarus.2010.02.010)
- Clarke, C. J., & Pringle, J. E. 1988, *MNRAS*, 235, 365, doi: [10.1093/mnras/235.2.365](https://doi.org/10.1093/mnras/235.2.365)
- de Vries, B. L., Acke, B., Blommaert, J. A. D. L., et al. 2012, *Nature*, 490, 74, doi: [10.1038/nature11469](https://doi.org/10.1038/nature11469)
- Desch, S. J., Estrada, P. R., Kalyaan, A., & Cuzzi, J. N. 2017, *ApJ*, 840, 86, doi: [10.3847/1538-4357/aa6bfb](https://doi.org/10.3847/1538-4357/aa6bfb)
- Desch, S. J., Kalyaan, A., & O'D. Alexander, C. M. 2018, *ApJS*, 238, 11, doi: [10.3847/1538-4365/aad95f](https://doi.org/10.3847/1538-4365/aad95f)
- Dong, R., Zhu, Z., & Whitney, B. 2015, *ApJ*, 809, 93, doi: [10.1088/0004-637X/809/1/93](https://doi.org/10.1088/0004-637X/809/1/93)
- Drążkowska, J., Alibert, Y., & Moore, B. 2016, *A&A*, 594, A105, doi: [10.1051/0004-6361/201628983](https://doi.org/10.1051/0004-6361/201628983)
- Dullemond, C. P., Apai, D., & Walch, S. 2006, *ApJL*, 640, L67, doi: [10.1086/503100](https://doi.org/10.1086/503100)
- Ercolano, B., & Pascucci, I. 2017, *Royal Society Open Science*, 4, 170114, doi: [10.1098/rsos.170114](https://doi.org/10.1098/rsos.170114)
- Fukagawa, M., Tsukagoshi, T., Momose, M., et al. 2013, *PASJ*, 65, L14, doi: [10.1093/pasj/65.6.L14](https://doi.org/10.1093/pasj/65.6.L14)
- Fukai, R., & Arakawa, S. 2021, *ApJ*, 908, 64, doi: [10.3847/1538-4357/abd2b9](https://doi.org/10.3847/1538-4357/abd2b9)
- Gail, H. P. 2001, *A&A*, 378, 192, doi: [10.1051/0004-6361:20011130](https://doi.org/10.1051/0004-6361:20011130)
- Haghighipour, N., & Boss, A. P. 2003, *ApJ*, 583, 996, doi: [10.1086/345472](https://doi.org/10.1086/345472)
- Hallenbeck, S. L., Nuth, Joseph A., I., & Nelson, R. N. 2000, *ApJ*, 535, 247, doi: [10.1086/308810](https://doi.org/10.1086/308810)
- Hanner, M. S., Brooke, T. Y., & Tokunaga, A. T. 1995, *ApJ*, 438, 250, doi: [10.1086/175069](https://doi.org/10.1086/175069)
- Harker, D. E., & Desch, S. J. 2002, *ApJL*, 565, L109, doi: [10.1086/339363](https://doi.org/10.1086/339363)
- Hartmann, L., Calvet, N., Gullbring, E., & D'Alessio, P. 1998, *ApJ*, 495, 385, doi: [10.1086/305277](https://doi.org/10.1086/305277)
- Honda, M., Kataza, H., Okamoto, Y. K., et al. 2003, *ApJL*, 585, L59, doi: [10.1086/374034](https://doi.org/10.1086/374034)
- Honda, M., Watanabe, J.-i., Yamashita, T., et al. 2004, *ApJ*, 601, 577, doi: [10.1086/380478](https://doi.org/10.1086/380478)
- Honda, M., Kataza, H., Okamoto, Y. K., et al. 2006, *ApJ*, 646, 1024, doi: [10.1086/505035](https://doi.org/10.1086/505035)
- Hughes, A. L. H., & Armitage, P. J. 2010, *ApJ*, 719, 1633, doi: [10.1088/0004-637X/719/2/1633](https://doi.org/10.1088/0004-637X/719/2/1633)
- Johansen, A., Blum, J., Tanaka, H., et al. 2014, in *Protostars and Planets VI*, ed. H. Beuther, R. S. Klessen, C. P. Dullemond, & T. Henning, 547, doi: [10.2458/azu_uapress_9780816531240-ch024](https://doi.org/10.2458/azu_uapress_9780816531240-ch024)
- Johansen, A., & Klahr, H. 2005, *ApJ*, 634, 1353, doi: [10.1086/497118](https://doi.org/10.1086/497118)
- Juhász, A., Bouwman, J., Henning, T., et al. 2010, *ApJ*, 721, 431, doi: [10.1088/0004-637X/721/1/431](https://doi.org/10.1088/0004-637X/721/1/431)
- Kanagawa, K. D., Muto, T., Okuzumi, S., et al. 2018, *ApJ*, 868, 48, doi: [10.3847/1538-4357/aae837](https://doi.org/10.3847/1538-4357/aae837)
- Keller, C., & Gail, H. P. 2004, *A&A*, 415, 1177, doi: [10.1051/0004-6361:20034629](https://doi.org/10.1051/0004-6361:20034629)
- Kemper, F., Vriend, W. J., & Tielens, A. G. G. M. 2004, *ApJ*, 609, 826, doi: [10.1086/421339](https://doi.org/10.1086/421339)
- Lambrechts, M., & Johansen, A. 2014, *A&A*, 572, A107, doi: [10.1051/0004-6361/201424343](https://doi.org/10.1051/0004-6361/201424343)

- Lynden-Bell, D., & Pringle, J. E. 1974, *MNRAS*, 168, 603, doi: [10.1093/mnras/168.3.603](https://doi.org/10.1093/mnras/168.3.603)
- Maaskant, K. M., de Vries, B. L., Min, M., et al. 2015, *A&A*, 574, A140, doi: [10.1051/0004-6361/201423770](https://doi.org/10.1051/0004-6361/201423770)
- Miura, H., Tanaka, K. K., Yamamoto, T., et al. 2010, *ApJ*, 719, 642, doi: [10.1088/0004-637X/719/1/642](https://doi.org/10.1088/0004-637X/719/1/642)
- Miyake, T., Suzuki, T. K., & Inutsuka, S.-i. 2016, *ApJ*, 821, 3, doi: [10.3847/0004-637X/821/1/3](https://doi.org/10.3847/0004-637X/821/1/3)
- Mousis, O., Petit, J. M., Wurm, G., et al. 2007, *A&A*, 466, L9, doi: [10.1051/0004-6361:20077170](https://doi.org/10.1051/0004-6361:20077170)
- Ogliore, R. C., Westphal, A. J., Gainsforth, Z., et al. 2009, *Meteoritics and Planetary Science*, 44, 1675, doi: [10.1111/j.1945-5100.2009.tb01198.x](https://doi.org/10.1111/j.1945-5100.2009.tb01198.x)
- Ohashi, S., Kobayashi, H., Nakatani, R., et al. 2021, *ApJ*, 907, 80, doi: [10.3847/1538-4357/abd0fa](https://doi.org/10.3847/1538-4357/abd0fa)
- Okuzumi, S., Momose, M., Sirono, S.-i., Kobayashi, H., & Tanaka, H. 2016, *ApJ*, 821, 82, doi: [10.3847/0004-637X/821/2/82](https://doi.org/10.3847/0004-637X/821/2/82)
- Okuzumi, S., Tanaka, H., Kobayashi, H., & Wada, K. 2012, *ApJ*, 752, 106, doi: [10.1088/0004-637X/752/2/106](https://doi.org/10.1088/0004-637X/752/2/106)
- Okuzumi, S., & Tazaki, R. 2019, *ApJ*, 878, 132, doi: [10.3847/1538-4357/ab204d](https://doi.org/10.3847/1538-4357/ab204d)
- Ootsubo, T., Watanabe, J.-i., Kawakita, H., Honda, M., & Furusho, R. 2007, *Planet. Space Sci.*, 55, 1044, doi: [10.1016/j.pss.2006.11.012](https://doi.org/10.1016/j.pss.2006.11.012)
- Ormel, C. W., & Cuzzi, J. N. 2007, *A&A*, 466, 413, doi: [10.1051/0004-6361:20066899](https://doi.org/10.1051/0004-6361:20066899)
- Pavlyuchenkov, Y., & Dullemond, C. P. 2007, *A&A*, 471, 833, doi: [10.1051/0004-6361:20077317](https://doi.org/10.1051/0004-6361:20077317)
- Pinilla, P., Pohl, A., Stammer, S. M., & Birnstiel, T. 2017, *ApJ*, 845, 68, doi: [10.3847/1538-4357/aa7edb](https://doi.org/10.3847/1538-4357/aa7edb)
- Sekiya, M., & Onishi, I. K. 2018, *ApJ*, 860, 140, doi: [10.3847/1538-4357/aac4a7](https://doi.org/10.3847/1538-4357/aac4a7)
- Shakura, N. I., & Sunyaev, R. A. 1973, *A&A*, 500, 33
- Sturm, B., Bouwman, J., Henning, T., et al. 2013, *A&A*, 553, A5, doi: [10.1051/0004-6361/201220243](https://doi.org/10.1051/0004-6361/201220243)
- Suzuki, T. K., & Inutsuka, S.-i. 2009, *ApJL*, 691, L49, doi: [10.1088/0004-637X/691/1/L49](https://doi.org/10.1088/0004-637X/691/1/L49)
- Suzuki, T. K., Muto, T., & Inutsuka, S.-i. 2010, *ApJ*, 718, 1289, doi: [10.1088/0004-637X/718/2/1289](https://doi.org/10.1088/0004-637X/718/2/1289)
- Suzuki, T. K., Ogihara, M., Morbidelli, A., Crida, A., & Guillot, T. 2016, *A&A*, 596, A74, doi: [10.1051/0004-6361/201628955](https://doi.org/10.1051/0004-6361/201628955)
- Takahashi, S. Z., & Inutsuka, S.-i. 2014, *ApJ*, 794, 55, doi: [10.1088/0004-637X/794/1/55](https://doi.org/10.1088/0004-637X/794/1/55)
- Takahashi, S. Z., & Muto, T. 2018, *ApJ*, 865, 102, doi: [10.3847/1538-4357/aadda0](https://doi.org/10.3847/1538-4357/aadda0)
- Taki, T., Kuwabara, K., Kobayashi, H., & Suzuki, T. K. 2021, *ApJ*, 909, 75, doi: [10.3847/1538-4357/abd79f](https://doi.org/10.3847/1538-4357/abd79f)
- Tanaka, K. K., Yamamoto, T., & Kimura, H. 2010, *ApJ*, 717, 586, doi: [10.1088/0004-637X/717/1/586](https://doi.org/10.1088/0004-637X/717/1/586)
- Tazaki, R., & Nomura, H. 2015, *ApJ*, 799, 119, doi: [10.1088/0004-637X/799/2/119](https://doi.org/10.1088/0004-637X/799/2/119)
- Testi, L., Birnstiel, T., Ricci, L., et al. 2014, in *Protostars and Planets VI*, ed. H. Beuther, R. S. Klessen, C. P. Dullemond, & T. Henning, 339, doi: [10.2458/azu_uapress_9780816531240-ch015](https://doi.org/10.2458/azu_uapress_9780816531240-ch015)
- Tominaga, R. T., Takahashi, S. Z., & Inutsuka, S.-i. 2019, *ApJ*, 881, 53, doi: [10.3847/1538-4357/ab25ea](https://doi.org/10.3847/1538-4357/ab25ea)
- Tsukagoshi, T., Nomura, H., Muto, T., et al. 2016, *ApJL*, 829, L35, doi: [10.3847/2041-8205/829/2/L35](https://doi.org/10.3847/2041-8205/829/2/L35)
- Ueda, T., Flock, M., & Okuzumi, S. 2019, *ApJ*, 871, 10, doi: [10.3847/1538-4357/aaf3a1](https://doi.org/10.3847/1538-4357/aaf3a1)
- van Boekel, R., Henning, T., Menu, J., et al. 2017, *ApJ*, 837, 132, doi: [10.3847/1538-4357/aa5d68](https://doi.org/10.3847/1538-4357/aa5d68)
- Vinković, D. 2009, *Nature*, 459, 227, doi: [10.1038/nature08032](https://doi.org/10.1038/nature08032)
- Yamamoto, D., & Tachibana, S. 2018, *ACS Earth and Space Chemistry*, 2, 778, doi: [10.1021/acsearthspacechem.8b00047](https://doi.org/10.1021/acsearthspacechem.8b00047)
- Yang, C. C., Johansen, A., & Carrera, D. 2017, *A&A*, 606, A80, doi: [10.1051/0004-6361/201630106](https://doi.org/10.1051/0004-6361/201630106)
- Yang, L., & Ciesla, F. J. 2012, *Meteoritics and Planetary Science*, 47, 99, doi: [10.1111/j.1945-5100.2011.01315.x](https://doi.org/10.1111/j.1945-5100.2011.01315.x)
- Youdin, A. N., & Lithwick, Y. 2007, *Icarus*, 192, 588, doi: [10.1016/j.icarus.2007.07.012](https://doi.org/10.1016/j.icarus.2007.07.012)